Robust Feature Detection for Signal Interception

Chad M. Spooner, *Member, IEEE,* and William A. Gardner, *Fellow, IEEE*

Abstract— **The problem of detecting the presence of direct sequence spread-spectrum signals in noise is considered, and the detector consisting of a filter followed by a delay-and-multiply device is optimized with respect to the filter bandwidth and the delay to maximize robustness to errors in assumed values of pulse rate and carrier frequency. Output SNR is used for performance optimization, and the results are corroborated by evaluating receiver operating characteristics.**

I. Introduction

THE PURPOSE of this paper is to present the results of a study of the robustness of the quadratic detector consisting of a filter followed by a delay-and-multiply device that multiplies the filtered signal by a delayed and conjugated replica of itself. This delay-and-multiply (DM) detector is commonly used to regenerate a spectral line at a frequency equal to the pulse rate of a PCM signal for purposes of detection of the signal's presence [1]–[5], [10] or synchronization to the signal's pulse timing phase [6]–[9]. Optimizing the DM detector with respect to the filter bandwidth and the delay requires knowledge of the pulse rate and carrier frequency. When the pulse rate or carrier frequency assumed for optimization is in error, the bandwidth and/or delay that maximizes detection performance for the erroneous pulse rate or carrier frequency is suboptimum for the actual pulse rate and carrier frequency. This suggests maximizing the robustness of the detector, as measured by the degree of tolerance to error in pulse rate and carrier frequency.

In this paper, both output SNR and receiver operating characteristics (ROC's) are used as measures of performance for studying the robustness of the DM detector for baseband PCM signals, modeled as real PAM, and passband PCM signals (digital QAM, BPSK, QPSK), modeled as complex PAM, in white Gaussian noise (WGN). Since the primary application motivating this work is detection of spread-spectrum signals in noise, only low-SNR conditions are considered. Furthermore, low-SNR conditions give rise to some simplifications in the theory.

To put the DM detector in perspective, it is pointed out that the weak-signal likelihood-ratio detector for PAM in WGN is a matched filter followed by a magnitude squarer [1]. This detector also maximizes the output SNR (as defined in Section II) for the regenerated spectral line at the pulse-rate frequency [8]. This detector is the special case of the DM detector for which the prefilter is the matched filter and the delay is zero. This detector, however, is shown to be not as robust to errors in pulse rate and carrier frequency as that which is optimized for robustness.

In [10] the problem of detecting the presence of a distortionless perfectly down-converted BPSK signal (viz., a real PAM signal whose pulse transform is real) by using a DM device is studied. An output SNR is evaluated there and used to determine several optimum prefilter-and-delay structures, as well as to determine optimum bandwidths for rectangular prefilters for a small set of delays. The effect of an error in the knowledge of the pulse rate on the performance of these detectors is found in terms of output SNR and some approximate formulas for the probabilities of detection and false alarm are derived.

This paper[1] generalizes on the work in [10] by 1) *jointly* optimizing the delay and rectangular prefilter bandwidth parameters with respect to two distinct optimality criteria that are aimed at maximizing robustness to error in signal parameter values; 2) considering the general bandpass (or complex baseband) case as well as the real baseband case; 3) considering the effect of errors in the knowledge of the demodulated carrier offset (or carrier frequency); and 4) performing simulations to estimate the detection and false-alarm probabilities corresponding to the various detectors. The relationship between detection by spectral line generation and the theory of cyclostationary time-series is also clarified.

In [3]–[5] the related problem of designing the signal (i.e., designing the pulse shape and the distribution of the symbol sequence) to reduce detectability by reducing the strength of the spectral line that can be generated at the pulse-rate frequency is addressed.

In Section II, the signal models are defined, and the output SNR for a regenerated spectral line is defined and expressed explicitly in terms of the parameters of the signal, noise, and detector. This SNR is maximized in the Appendix for both the real PAM and complex PAM models. In Section III, the SNR is used to study the optimization of the filter bandwidth and the delay, and to evaluate the effects of errors in the values of pulse rate and carrier frequency used in the optimization. In Section IV the conclusions regarding detection performance are corroborated using ROC's obtained from simulations.

Paper approved by C. N. Georghiades, the Editor for Synchronization and Optical Detection of the IEEE Communications Society. Manuscript received March 15, 1991; revised July 28, 1992.

The authors are with the Department of Electrical and Computer Engineering, University of California at Davis, Davis, CA 95616.

IEEE Log Number 9213529.

[1] The work reported in this paper was conducted prior to the appearance of [10] in the literature, which occurred almost simultaneously with the submission of this paper for review for publication.

II. Output SNR Formulas

A. Signal Models

The model for a real baseband PAM signal is

$$s(t) = \sum_{n=-\infty}^{\infty} a_n p(t - nT_0 - \theta) \tag{1}$$

where $p(t)$ is the pulse, $\{a_n\}$ is a zero-mean, independent, and identically distributed symbol sequence, and $1/T_0$ and θ are the pulse rate and phase, respectively. For spread-spectrum signals, this model for $\{a_n\}$ is admittedly only approximate. For example, for a binary direct-sequence spread-spectrum signal, $\{a_n\}$ is actually the modulo-two sum of the high-rate spreading code sequence and the low-rate message symbol sequence. Also, for spread-spectrum signals, unlike bandwidth-efficient PCM, $p(t)$ has large excess bandwidth (bandwidth in excess of the minimum bandwidth for zero intersymbol interference) and can be usefully approximated as a rectangular pulse

$$p(t) = \begin{cases} 1, & |t| \le T_0/2 \\ 0, & |t| > T_0/2 \,. \end{cases} \tag{2}$$

In this case, the complex counterpart of model (1) applies to the complex envelope of both digital QAM and PSK signals (for which the phase-keying envelope is rectangular). For this passband signal model, $p(t)$ and $\{a_n\}$ are both complex-valued in order to accommodate any carrier offset, say f_0, and lack of Hermitian symmetry of the baseband pulse transform, as well as to accommodate the in-phase and quadrature symbol sequences. For example, for the real digital QAM signal

$$\begin{aligned} s(t) = &\sum_n c_n q(t - nT_0 - \theta)\cos(2\pi f_0 t - \varphi) \\ &+ \sum_m s_m q(t - mT_0 - \theta)\sin(2\pi f_0 t - \varphi) \end{aligned} \tag{3}$$

we have the complex envelope (1) with

$$a_n = (c_n + is_n)e^{i(2\pi n T_0 f_0 - \varphi)} \tag{4}$$

and

$$p(t) = q(t)e^{i2\pi f_0 t} \,. \tag{5}$$

It should be clarified that the model for $s(t)$ can be complex-valued even when the carrier frequency f_0 is known (which implies that perfect downconversion is possible) because, for instance, the channels's impulse response can force the spectrum to be asymmetrical about the carrier frequency, which results in a complex-valued baseband pulse in the complex-envelope model.

The complex envelope of the input to the detector consists of the signal (1) plus complex WGN

$$x(t) = s(t) + n(t) \,, \tag{6}$$

The output of the detector is given by

$$n(t) = n_c(t) + in_s(t) \,. \tag{7}$$

$$y(t) = w(t)w^*(t - d) \tag{8}$$

where $w(t)$ is the filtered input

$$w(t) = x(t) \otimes h(t) \tag{9}$$

and $h(t)$ is the impulse response of the filter preceding the delay-and-multiply device. From (6)–(9), we see that the output

$$\begin{aligned} y(t) = &[s(t) \otimes h(t)][s(t - d) \otimes h(t - d)]^* \\ &+ [s(t) \otimes h(t)][n(t - d) \otimes h(t - d)]^* \\ &+ [n(t) \otimes h(t)][s(t - d) \otimes h(t - d)]^* \\ &+ [n(t) \otimes h(t)][n(t - d) \otimes h(t - d)]^* \end{aligned} \tag{10}$$

consists of signal-only, noise-only, and signal-cross-noise terms. For the case of a weak signal, we can ignore the cross terms in defining the output SNR; that is, we can compute the output signal strength from the signal-only term and the output noise strength (approximately) from the noise-only term.

B. Output SNR

Since the sequence $\{a_n\}$ has zero mean value, then $s(t)$ does not contain any spectral lines. However, the output signal-only term will in general contain spectral lines at the pulse rate and its harmonics $k/T_0, k = \pm 1, \pm 2, \cdots$. The output signal strength is defined to be the time-averaged power of one of these regenerated spectral lines

$$P_s \triangleq \left| \left\langle [s(t) \otimes h(t)][s(t - d) \otimes h(t - d)]^* e^{-i2\pi\alpha t} \right\rangle \right|^2 \tag{11}$$

where $\langle \cdot \rangle$ denotes average over all time t, and $\alpha = k/T_0$.

The output-noise strength is defined to be the time-averaged power in a very narrow band of width B_α, centered at frequency α, due to the noise-only term

$$\begin{aligned} P_n &\triangleq \int_{\alpha - B/2}^{\alpha + B/2} S_m(f)\, df \\ &\cong B_\alpha S_m(\alpha) \end{aligned}$$

where $m(t)$ is the noise-only term

$$m(t) \triangleq [n(t) \otimes h(t)][n(t - d) \otimes h(t - d)]^* \tag{12}$$

and $S_m(f)$ is its spectral density of the time-averaged power.

The output SNR is then given by

$$\text{SNR} \triangleq \frac{P_s}{P_n} \,. \tag{13}$$

For the real signal and noise model (1) (with $\{a_n\}$, $p(t)$, and $n(t)$ real), it is shown in the Appendix that

$$\begin{aligned} \text{SNR} = \frac{\sigma_a^4}{T_0^2} \Bigg| &\int_{-\infty}^{\infty} H(f + \alpha/2)H^*(f - \alpha/2) \\ &\times P(f + \alpha/2)P^*(f - \alpha/2)e^{i2\pi f d}\, df \Bigg|^2 \\ \div\, 2B_\alpha &\int_{-\infty}^{\infty} \cos^2(2\pi f d)|H(f + \alpha/2)H^*(f - \alpha/2)|^2 \\ &\times S_n(f + \alpha/2)S_n(f - \alpha/2)\, df \,. \end{aligned} \tag{14}$$

For the complex signal and noise model (1) (with $\{a_n\}$, $p(t)$, and $n(t) = n_c(t) + in_s(t)$ complex), it is also shown in the Appendix that

$$\text{SNR} = \frac{\sigma_a^4}{T_0^2} \left| \int_{-\infty}^{\infty} H(f+\alpha/2)H^*(f-\alpha/2) \times P(f+\alpha/2)P^*(f-\alpha/2)e^{i2\pi fd}\,df \right|^2 \div 4B_\alpha \int_{-\infty}^{\infty} |H(f+\alpha/2)H^*(f-\alpha/2)|^2 \times S_{n_c}(f+\alpha/2)S_{n_c}(f-\alpha/2)\,df. \quad (15)$$

In (14) and (15) σ_a^2 is the temporal variance of the zero-mean sequence $\{a_n\}$:

$$\sigma_a^2 = \lim_{K\to\infty} \frac{1}{2K+1} \sum_{k=-K}^{K} |a_k|^2.$$

It is further shown in the Appendix that the SNR (14) for the real signal is maximum with respect to $H(f)$ if a solution to

$$H(f+\alpha/2)H^*(f-\alpha/2) \propto \frac{P^*(f+\alpha/2)P(f-\alpha/2)e^{-i2\pi fd}}{\cos^2(2\pi fd)S_n(f+\alpha/2)S_n(f-\alpha/2)} \quad (16)$$

exists; for $d = 0$, the solution is

$$H(f) = \frac{P^*(f)}{S_n(f)}. \quad (17)$$

This is recognized as the matched filter for the pulse $p(t)$ in noise with power spectral density $S_n(f)$. This optimum DM detector—the matched-filter squarer (MFS)—is identical to the optimum (maximum SNR for regenerated spectral line) among all quadratic detectors—not just those of the filter-and-delay-and-multiply form [8], [9].

Similarly, it is shown in the Appendix that the SNR (15) for the complex signal is maximum with respect to $H(f)$ if a solution to

$$H(f+\alpha/2)H^*(f-\alpha/2) \propto \frac{P^*(f+\alpha/2)P(f-\alpha/2)e^{-i2\pi fd}}{S_{n_c}(f+\alpha/2)S_{n_c}(f-\alpha/2)} \quad (18)$$

exists and again, for $d = 0$, we obtain the matched filter solution

$$H(f) = \frac{P^*(f)}{S_{n_c}(f)}. \quad (19)$$

Before proceeding, the relationship between the DM detector and the more general class of cyclic feature detectors that exploit the spectral correlation property that is characteristic of cyclostationary signals, as described in [1], is clarified. If we try to detect the presence of a regenerated spectral line at frequency α in the output of the DM detector by measuring the strength (Fourier coefficient) of the sine-wave component with frequency α in the output, then the detection statistic becomes

$$Z = \left| \frac{1}{T} \int_0^T [x(t) \otimes h(t)][x(t-d) \otimes h(t-d)]^* e^{-i2\pi\alpha t}\,dt \right|. \quad (20)$$

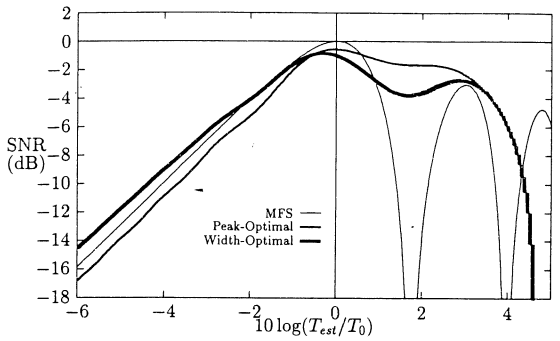

Fig. 1. Robustness to error in T_0 for peak-optimal and width-optimal bandwidth B and delay d in the delay-and-multiply (DM) detector, and for the matched-filter-squarer (MFS) detector, for real PAM.

This statistic can be re-expressed as

$$Z = \left| \int_{-\infty}^{\infty} S_x^\alpha(f)_T W^\alpha(f) e^{i2\pi d(f-\alpha/2)}\,df \right| \quad (21)$$

where $S_x^\alpha(f)_T$ is an estimate of the spectral correlation function or cyclic spectrum of $x(t)$ obtained by Fourier transforming the estimate of the cyclic autocorrelation of $x(t)$

$$R_x^\alpha(\tau)_T = \frac{1}{T} \int_0^T x(t+\tau/2)x^*(t-\tau/2)e^{-i2\pi\alpha t}\,dt \quad (22)$$

and where $W^\alpha(f)$ is given by

$$W^\alpha(f) = H(f+\alpha/2)H^*(f-\alpha/2) \quad (23)$$

which plays the role of a spectral smoothing window in (21).

When $d = 0$ and $H(f)$ is the matched filter (17) or (19), then (21) is identical to the optimum feature detector described in [1].

III. Robustness Evaluation and Optimization

The usual approach to optimizing a detector, such as the DM detector, is to ignore possible errors in parameters such as the pulse rate and to simply maximize a performance measure such as SNR for some nominal parameter value. Following this approach first, we adopt an idealized filter with rectangular passband and one-sided bandwidth B, and we maximize the SNR (14) or (15) with respect to both the delay d and the bandwidth B. The resultant peak-optimal detector exhibits the SNR versus pulse-rate error performance shown in Fig. 1 (cf. [10], Figs. 5 and 6] for the real PAM model and in Fig. 4 for the complex PAM model. The peak-optimal values of bandwidth and the resultant peak SNR versus delay are shown in Fig. 2 for real PAM and in Fig. 5 for complex PAM.

As an alternative to the preceding approach, to obtain a detector that is more robust to errors in the assumed value

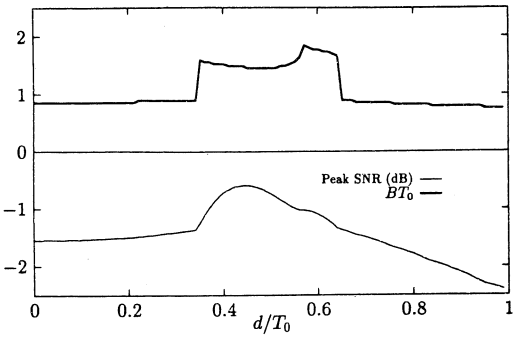

Fig. 2. Peak-optimal bandwidth B and peak SNR for the DM detector versus delay d for real PAM. The vertical axis is in decibels for peak SNR and is dimensionless for BT_0.

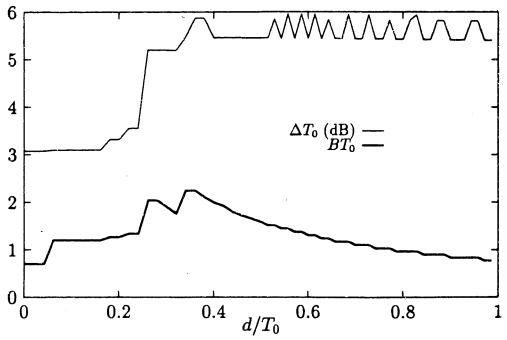

Fig. 3. Width-optimal bandwidth B and pulse-rate tolerance ΔT_0 for the DM detector versus delay d for real PAM. ΔT_0 is the -3dB-width of the peak-SNR versus pulse-rate-error curve (see, for example, Fig. 1).

of pulse rate, we maximize the -3-dB width of the SNR versus pulse-rate error performance curve with respect to the delay d and bandwidth B. The resultant width-optimal detector exhibits the SNR versus pulse-rate error performance shown in Fig. 1 for real PAM and in Fig. 4 for complex PAM. The width-optimal values of bandwidth B and the resultant tolerance (-3-dB width of SNR versus pulse-rate curve) to pulse-rate error versus delay d are shown in Fig. 3 for real PAM and in Fig. 6 for complex PAM.

The results in Figs. 1–6 were obtained for a signal and noise model with the following parameters:

$$\begin{aligned} \sigma_a &= 1 \\ S_n(f) \equiv 1 \quad &\text{or} \quad S_{n_c}(f) \equiv 1 \\ f_0 &= 1/4T_s \\ T_0 &= 16T_s \end{aligned} \tag{24}$$

where T_s is the sampling increment for a discrete-time implementation, and f_0 is the carrier-frequency offset in the downconverted complex PAM model. The spectral line frequency α used was the pulse rate $1/T_0$. (Note: The jagged appearance of the curves in Figs. 2, 3, and 6 is a result of the fact that the optimization search was over discretized versions of the parameters d, B, T_{est}).

For real PAM, it can be seen from Fig. 2 that

$$\begin{aligned} d &= 0.45T_0 \\ B &= 1.445/T_0 \end{aligned}$$

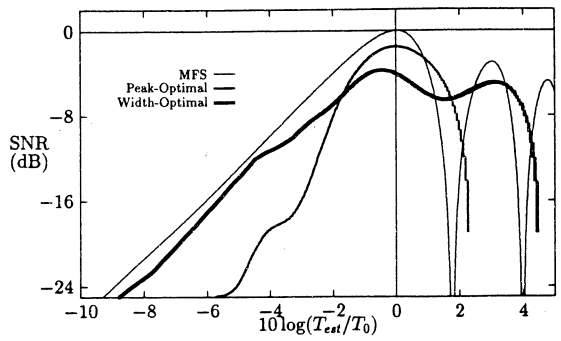

Fig. 4. Robustness to error in T_0 for the DM detector with peak-optimal and width-optimal bandwidth B and delay d, and for the MFS detector, for complex PAM.

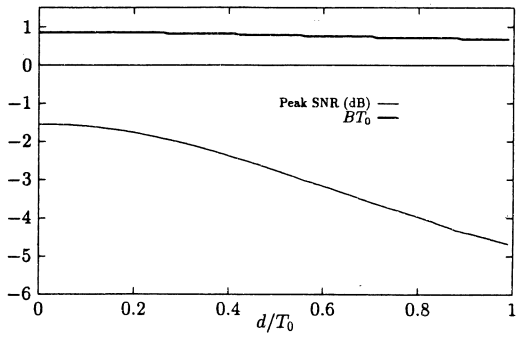

Fig. 5. Peak-optimal bandwidth B and peak SNR for the DM detector versus delay d for complex PAM.

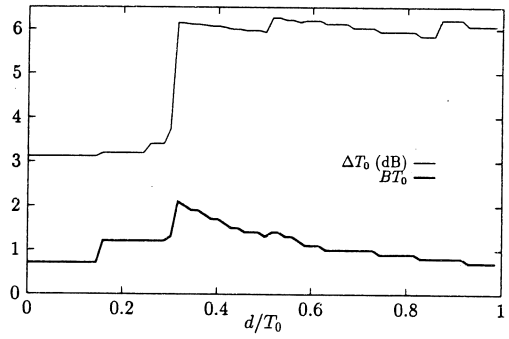

Fig. 6. Width-optimal bandwidth B and pulse-rate tolerance ΔT_0 for the DM detector versus delay d for complex PAM.

are the jointly peak-optimal detector parameters and, from Fig. 1, these parameter values result in an SNR that is only 0.6 dB below that of the optimum (MFS) detector, which is used as a reference (0-dB SNR). From Fig. 3, it can be seen that

$$\begin{aligned} d &= 0.557T_0 \\ B &= 1.452/T_0 \end{aligned}$$

are the joint width-optimal detector parameters for real PAM, and from Fig. 1 it follows that the width-optimal detector, by comparison with the peak-optimal, provides up to 2 dB more SNR for pulse rates $1/T_0$ that are lower than the expected rate $1/T_{\text{est}}[\log(T_{\text{est}}/T_0) < 0]$, but also results in up to 2 dB less SNR for some pulse rates that are higher than expected. Although the peak value of width-optimal SNR is 1.7 dB

below that of the optimum MFS detector, both the peak-optimal and width-optimal detectors are far superior to the MFS for some pulse rates that are higher than expected, whereas they are comparable to the MFS for pulse rates that are lower than expected.

A practical compromise between the peak-optimal and width-optimal parameter values is $d = T_0/2$ and $B = 1.5/T_0$.

For complex PAM, the results are a little more interesting. It follows from Fig. 5 that the peak-optimal parameter values are

$$d = 0$$
$$B = 0.85/T_0$$

and we can see from Fig. 4 that this results in an SNR that is 1.55 dB lower than that provided by the optimum MFS detector. From Fig. 4, it follows that

$$d = 0.52T_0$$
$$B = 1.40/T_0$$

are the width-optimal parameter values, and Fig. 4 shows that the width-optimal detector provides up to 10 dB more SNR than the peak-optimal detector for pulse rates that are lower than expected and even more than 10-dB improvement for higher pulse rates. However, this results in 2.65-dB loss relative to the peak-optimal and 4.2-dB loss relative to the optimal MFS detector when there is no error in the expected pulse rate. On the other hand, the MFS detector can perform quite poorly compared with the width-optimal detector when the actual pulse rate is higher than expected.

The robustness optimization for complex signals was done for the case of a real-valued pulse and a perfect match between the filter's center frequency and the signal's center frequency. In this case, the pulse-rate line appears in the real portion of the delay-and-multiply product. The complex statistic is nevertheless used because it provides a best case complex-signal robustness evaluation: for any other case, a specific complex pulse (channel impulse response) or carrier mismatch must be chosen.

In addition, Fig. 7 shows the robustness of the three detectors to errors in the assumed value of carrier offset for complex PAM signals. The data in this figure were generated by evaluating the SNR's for the case of a mismatch between the center frequency of the filter and the center frequency of the signal's power spectrum (the center of $P(f)$ does not match the center of $H(f)$). Although the peak-optimal and MFS detectors exhibit similar degradations due to this type of error, the width-optimal detector is substantially more tolerant.

In summary, by accepting a few decibel loss in SNR for the best case of no error in the assumed pulse rate or carrier frequency for complex PAM, we can obtain substantial improvements in tolerance to both of these errors when they are relatively large by using the width-optimal parameters values.

IV. Simulations

To corroborate the results and conclusions drawn in Section III on the basis of SNR, we show here a sampling of ROC's obtained for a BPSK signal with parameter values as

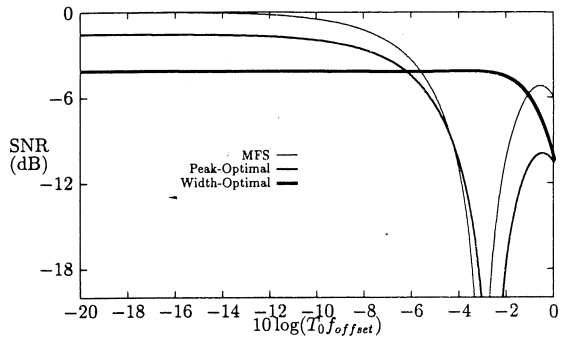

Fig. 7. Robustness to carrier offset error for the DM detector with peak-optimal and width-optimal bandwidth B and delay d, and for the MFS detector, for complex PAM.

specified in (24). Thus in the case of real signals, a baseband binary PAM signal with $T_0 = 16T_s$ is simulated, and in the case of complex signals, the same real signal is simulated and then modulated by a complex exponential with frequency $1/4T_s$.

For each ROC curve, 500 independent statistics for each hypothesis are computed. Each statistic is computed in the following way. The signal is generated (on the signal-present hypothesis only) and added to WGN that is simulated using an IMSL library routine. These data are filtered by the appropriate $H(f)$ and then multiplied by delayed versions of themselves. The ideal rectangular filter is implemented in the frequency domain by simply zeroing the appropriate bins in the FFT of the signal. The delay and the bandwidth of the filter are assumed to be specified in terms of the estimated value of the pulse rate and are therefore determined by T_{est}. An FFT is applied and the bin corresponding to $1/T_0$, the true pulse rate, is selected. The magnitude of this bin is the detection statistic. The value of the spectral density height for the noise changes from case to case (but remains constant for all the ROC's in a single figure).

Figs. 8 and 9 show ROC's for the MFS and peak-optimal detectors for real signals with $T_{\text{est}}/T_0 = 0.5$ (−3 dB) and 1.6 (1.9 dB), respectively. These ROC's show that the performance difference between the two detectors is correctly predicted by the separation between the SNR curves in Fig. 1. Figs. 10 and 11 show ROC's for the case of complex signals, using the same two values of T_{est}/T_0 as in the previous two figures. These figures validate the performance ordering given by the SNR curves in Fig. 4.

Figs. 12 and 13 show ROC's for all three complex-signal optimal detectors for the case of a carrier-offset error. That is, there is a mismatch between the signal's carrier offset and the center frequency of the pre-filter $H(f)$. In Fig. 12, this offset is 1% of the pulse rate $1/T_0$ and in Fig. 13, it is 2% of $1/T_0$. These ROC's corroborate the SNR curves in Fig. 7.

V. Conclusions

For real PAM signals, both the peak-optimal and width-optimal DM detectors offer enhanced tolerance, relative to the MFS detector, to error in the assumed value of the pulse rate of a signal to be detected when the actual value exceeds the assumed rate by more than 1 dB. However, for complex

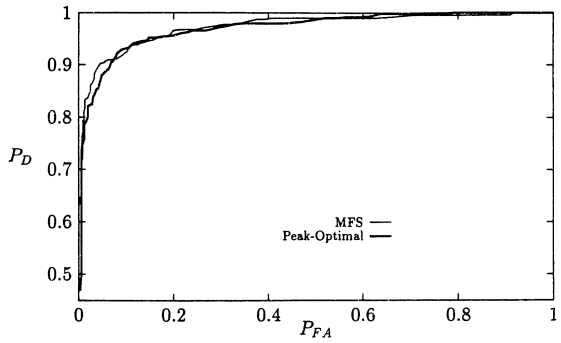

Fig. 8. Receiver operating characteristics (ROC's) for a real signal: $10\log(T_{\text{est}}/T_0) = -3$ dB.

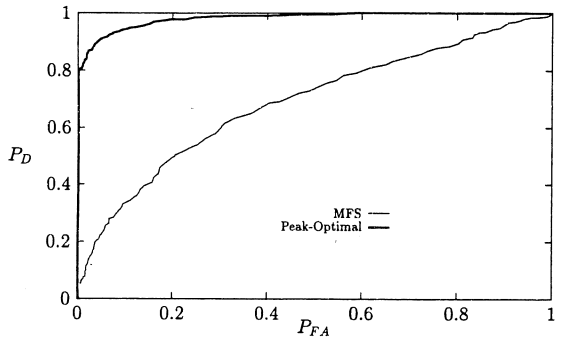

Fig. 9. ROC's for a real signal: $10\log(T_{\text{est}}/T_0) = 1.9$ dB.

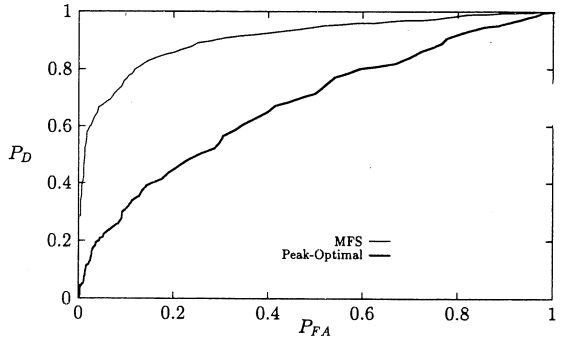

Fig. 10. ROC's for a complex signal: $10\log(T_{\text{est}}/T_0) = -3$ dB.

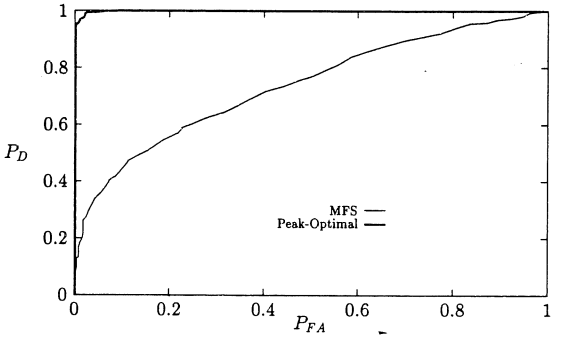

Fig. 11. ROC's for a complex signal: $10\log(T_{\text{est}}/T_0) = 1.9$ dB.

PAM signals, the peak-optimal detector performs quite poorly, whereas the width-optimal (or optimally robust) detector again provides enhanced tolerance to actual pulse rates that exceed the assumed rate by more than 1 dB. For actual pulse rates

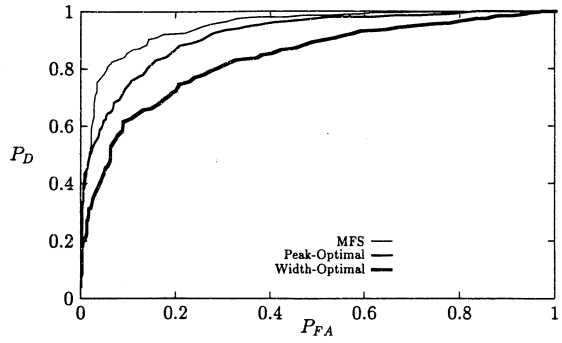

Fig. 12. ROC's for a complex signal: carrier offset error of $10\log(T_0 f_{\text{offset}}) = -8$ dB.

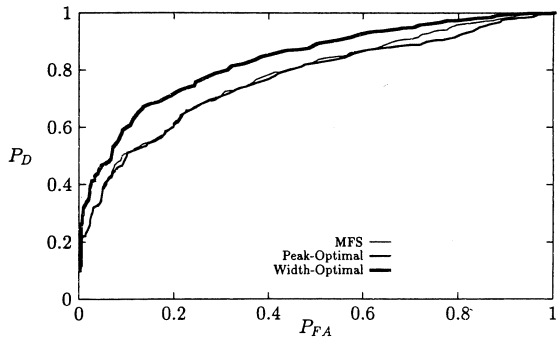

Fig. 13. ROC's for a complex signal: carrier offset error of $10\log(T_0 f_{\text{offset}}) = -5$ dB.

that are lower than the assumed rate, the width-optimal detector—compared with the MFS detector—can provide up to 2 dB higher SNR for real PAM but can be nearly 2 dB worse for complex PAM, and is as much as 4 dB worse when the pulse-rate error is between -1 and $+1$ dB for complex PAM. However, to offset this, the width-optimal detector performs well for carrier-offset errors (normalized by the pulse rate) as large as -1 dB, whereas the MFS detector fails for errors exceeding -5 dB.

In conclusion, by comparison with the optimum MFS detector, the optimally robust DM detector offers enhanced tolerance to errors in assumed values of pulse rate and carrier offset. However, if the objective is to design a detector that performs as well as possible for all possible carrier frequencies and pulse rates, then the prefilter/delay/multiply followed by a spectral-line detector is not necessarily the most appropriate quadratic device. The cyclic spectrum analyzer (also called the spectral correlation analyzer) [1], [9] provides more flexibility for search-type detection and, with linear postprocessing (weighted integration over frequency), can implement the optimum quadratic detectors for all possible carrier frequencies and pulse rates. Moreover, it can implement the optimum quadratic detector for any cyclostationary signal—not just the PSK signals considered in this paper—simply by choosing the appropriate linear postprocessing.

APPENDIX
SNR OPTIMIZATION

In this Appendix the performance measure SNR (13) is derived and maximized for a PAM signal in white Gaussian

noise. Recall that the SNR is given by

$$\text{SNR} = \frac{P_s}{P_n} = \frac{\left|\left\langle [s(t) \otimes h(t)][s(t-d) \otimes h(t-d)]^* e^{-i2\pi\alpha t}\right\rangle\right|^2}{B_\alpha S_m(\alpha)}, \tag{A1}$$

where $S_m(\alpha)$ is the PSD of the output of the DM with noise only at the input. The calculation of (A1) is split into numerator and denominator calculations.

Numerator Calculation

The signal model for $s(t)$ is given by (1). Let $b(t)$ denote the output of the DM with $s(t)$ at the input

$$b(t) = [s(t) \otimes h(t)][s(t-d) \otimes h(t-d)]^* \tag{A2}$$

$$= \sum_{n=-\infty}^{\infty} \sum_{m=-\infty}^{\infty} a_n a_m^* g(t - nT_0 - \theta) \tag{A3}$$

$$\times\, g^*(t - mT_0 - \theta - d)\,. \tag{A4}$$

In (A3), $g(t)$ is the filtered pulse

$$g(t) = p(t) \otimes h(t)\,. \tag{A4}$$

The value of $\langle b(t)e^{-i2\pi\alpha t}\rangle$ is sought. Starting with

$$\langle b(t)e^{-i2\pi\alpha t}\rangle = \lim_{K\to\infty} \frac{1}{(2K+1)T_0} \times \sum_{k=-K}^{K} \int_{-T_0/2}^{T_0/2} b(t + kT_0) e^{-i2\pi\alpha(t+kT_0)}\, dt \tag{A5}$$

and using (A3) yields the following relation:

$$\langle b(t)e^{-i2\pi\alpha t}\rangle = \lim_{K\to\infty} \frac{1}{(2K+1)T_0} \sum_{k=-K}^{K} \int_{-T_0/2}^{T_0/2} \times \sum_{n,m} a_n a_m^* g(t + kT_0 - nT_0 - \theta) \times g^*(t + kT_0 - mT_0 - \theta - d) e^{-i2\pi\alpha(t+kT_0)}\, dt\,. \tag{A6}$$

A change of summation indices for n and m and subsequent simplification yields

$$\langle b(t)e^{-i2\pi\alpha t}\rangle = \lim_{K\to\infty} \frac{1}{(2K+1)T_0} \times \int_{-T_0/2}^{T_0/2} \sum_{n',m'} \left(\sum_{k=-K}^{K} a_{k-n'} a_{k-m'}^* e^{-i2\pi\alpha k T_0} \right) \times g(t - n'T_0 - \theta) g^*(t - m'T_0 - \theta - d) e^{-i2\pi\alpha t}\, dt\,. \tag{A7}$$

Since the symbol sequence $\{a_n\}$ is independent and identically distributed, then

$$\lim_{K\to\infty} \frac{1}{(2K+1)T_0} \sum_{k=-K}^{K} a_{k-n'} a_{k-m'}^* e^{-i2\pi\alpha k T_0} = \begin{cases} \sigma_a^2, & m' = n', \alpha = p/T_0 \\ 0, & \text{otherwise}, \end{cases} \tag{A8}$$

where $p = 0, \pm 1, \pm 2, \cdots$. Therefore

$$\langle b(t)e^{-i2\pi\alpha t}\rangle = \frac{\sigma_a^2}{T_0} \int_{-T_0/2}^{T_0/2} \sum_n g(t - nT_0 - \theta) \times g^*(t - nT_0 - \theta - d) e^{-i2\pi\alpha t}\, dt, \tag{A9}$$

for $\alpha = p/T_0$. Expressing $g(t)$ in terms of its Fourier transform $G(f)$ and using the identity

$$\sum_{n=-\infty}^{\infty} e^{-i2\pi(f_1 - f_2)nT_0} = \frac{1}{T_0} \sum_{n=-\infty}^{\infty} \delta(f_1 - f_2 - nT_0) \tag{A10}$$

in (A9) yields

$$\langle b(t)e^{-i2\pi\alpha t}\rangle = \sum_{n=-\infty}^{\infty} \frac{\sigma_a^2}{T_0^2} \times \int_{-\infty}^{\infty} G(f + n/T_0) G^*(f) e^{i2\pi f d} e^{-i2\pi n\theta/T_0}\, df \times \int_{-T_0/2}^{T_0/2} e^{-i2\pi t(\alpha - n/T_0)}\, dt \tag{A11}$$

for $\alpha = p/T_0$. The second integral in (A11) vanishes for $n/T_0 \neq \alpha = p/T_0$ so that

$$\langle b(t)e^{-i2\pi\alpha t}\rangle = \frac{\sigma_a^2}{T_0} \int_{-\infty}^{\infty} P\left(f + \frac{\alpha}{2}\right) P^*\left(f - \frac{\alpha}{2}\right) \times H\left(f + \frac{\alpha}{2}\right) H^*\left(f - \frac{\alpha}{2}\right) e^{i2\pi f d}\, df\, e^{-i2\pi\alpha\theta} \tag{A12}$$

where $\alpha = p/T_0$, and $P(f)$ and $H(f)$ are the Fourier transforms of $p(t)$ and $h(t)$, respectively. Note that for even $G(f) = P(f)H(f)$, (A12) reduces to

$$\langle b(t)e^{-i2\pi\alpha t}\rangle = \frac{\sigma_a^2}{T_0} \int_{-\infty}^{\infty} P\left(f + \frac{\alpha}{2}\right) P^*\left(f - \frac{\alpha}{2}\right) H\left(f + \frac{\alpha}{2}\right) \times H^*\left(f - \frac{\alpha}{2}\right) \cos(2\pi f d)\, df\, e^{-i2\pi\alpha\theta}\,. \tag{A13}$$

Denominator Calculation

The noise is bandlimited and Gaussian, either lowpass (in the case of real signals) or bandpass (in the case of complex signals) and has a constant spectral height in its passband. In either case it is assumed that the noise $n(t)$ has the representation

$$n(t) = n_c(t)\cos(2\pi f_c t) - n_s(t)\sin(2\pi f_c t)\,. \tag{A14}$$

In the case of real signals, $f_c = 0$ and $n(t) \equiv n_c(t)$, whereas in the case of complex signals f_c can be taken to be the center frequency of the signal of interest. In either case, if we assume that the spectrum of the noise is symmetric about f_c, then the crosscorrelation between $n_c(t)$ and $n_s(t)$ is zero.

The input to the DM receiver is the complex envelope

$$n_r(t) = n_c(t) + in_s(t) \tag{A15}$$

and the corresponding output is $m(t)$. To find the PSD of $m(t)$, the autocorrelation is computed and then Fourier transformed. With $u(t) = n_r(t) \otimes h(t)$, the autocorrelation function for $m(t)$ is

$$R_m(\tau) = \langle u(t+\tau/2)u^*(t+\tau/2-d)u^*(t-\tau/2)u(t-\tau/2-d)\rangle\,. \tag{A16}$$

An application of Isserlis' formula [9] to (A16) yields

$$R_m(\tau) = |R_u(d)|^2 + |R_u(\tau)|^2 + R_{uu^*}(\tau+d)R^*_{uu^*}(\tau-d)\,. \tag{A17}$$

It is straightforward to show that

$$R_u(\tau) = \iint_{-\infty}^{\infty} h(\lambda)h(\gamma) \times [R_{n_c}(\tau-\lambda+\gamma) + R_{n_s}(\tau-\lambda+\gamma)]\,d\lambda\,d\gamma \tag{A18}$$

and that

$$R_{uu^*}(\tau) = \iint_{-\infty}^{\infty} h(\lambda)h(\gamma) \times [R_{n_c}(\tau-\lambda+\gamma) - R_{n_s}(\tau-\lambda+\gamma)]\,d\lambda\,d\gamma\,. \tag{A19}$$

The spectral density $S_m(\alpha)$ for $\alpha \neq 0$ is given by the Fourier transform of the last two terms in (A17). The special cases of real and complex signals are treated separately.

Real Signal: Here $n_s(t) \equiv 0$, which implies that $R_{n_s}(\tau) \equiv 0$. Thus the integrals in (A18) and (A19) are identical. The spectral density therefore becomes

$$S_m(\alpha) = 2\int_{-\infty}^{\infty} \cos^2(2\pi f d)\left|H^*\left(f-\frac{\alpha}{2}\right)H\left(f+\frac{\alpha}{2}\right)\right|^2 \times S_n\left(f+\frac{\alpha}{2}\right)S_n\left(f-\frac{\alpha}{2}\right)df\,. \tag{A20}$$

Complex Signal: Here $R_{n_c}(\tau) \equiv R_{n_s}(\tau)$, which implies that (A19) vanishes. The spectral density therefore becomes

$$S_m(\alpha) = 4\int_{-\infty}^{\infty} \left|H^*\left(f-\frac{\alpha}{2}\right)H\left(f+\frac{\alpha}{2}\right)\right|^2 \times S_{n_c}\left(f+\frac{\alpha}{2}\right)S_{n_c}\left(f-\frac{\alpha}{2}\right)df\,. \tag{A21}$$

Combining (A1), (A12), and (A20) yields the SNR (14) for real signals. Combining (A1), (A12), and (A21) yields the SNR (15) for complex signals.

The Ratio

To obtain the optimum SNR in (15), the numerator, which is the squared magnitude of (A12), is written as

$$\left|\int_{-\infty}^{\infty} e^{i2\pi fd}\,\frac{P\left(f+\frac{\alpha}{2}\right)P^*\left(f-\frac{\alpha}{2}\right)}{\sqrt{S_{n_c}\left(f+\frac{\alpha}{2}\right)S_{n_c}\left(f-\frac{\alpha}{2}\right)}} \times\sqrt{S_{n_c}\left(f+\frac{\alpha}{2}\right)S_{n_c}\left(f-\frac{\alpha}{2}\right)} \times H\left(f+\frac{\alpha}{2}\right)H^*\left(f-\frac{\alpha}{2}\right)df\right|^2$$

and the Schwarz inequality is applied. This leads to the sufficient optimal-filter design equation

$$H\left(f+\frac{\alpha}{2}\right)H^*\left(f-\frac{\alpha}{2}\right) \propto \frac{P^*\left(f+\frac{\alpha}{2}\right)P\left(f-\frac{\alpha}{2}\right)e^{-i2\pi fd}}{S_{n_c}\left(f+\frac{\alpha}{2}\right)S_{n_c}\left(f-\frac{\alpha}{2}\right)} \tag{A22}$$

for complex signals. The maximum SNR for real signals (14) can be obtained similarly. This results in the sufficient optimal-filter design equation

$$H\left(f+\frac{\alpha}{2}\right)H^*\left(f-\frac{\alpha}{2}\right) \propto \frac{P^*\left(f+\frac{\alpha}{2}\right)P\left(f-\frac{\alpha}{2}\right)e^{-i2\pi fd}}{\cos^2(2\pi fd)S_n\left(f+\frac{\alpha}{2}\right)S_n\left(f-\frac{\alpha}{2}\right)} \tag{A23}$$

for real signals. Equations (A22) and (A23) are only sufficient, not necessary, because the Schwartz inequality yields a maximum only when a solution to (A22) or (A23) exists. For example, for $d = 0$, solutions exists, but for $d \neq 0$, solutions do not necessarily exist. However, if $G(f) = P(f)H(f)$ turns out to be even, then using (A13) in place of (A12) results in the replacement of $e^{-i2\pi fd}$ in (A22) and (A23) with $\cos(2\pi fd)$. In this case, solutions do exist for some $d \neq 0$, e.g., $d = rM/2\alpha$ for odd integers r, since then $\cos(2\pi fd) = 2\cos(\pi(f+\alpha/2)d)\cos(\pi(f-\alpha/2)d)$.

REFERENCES

[1] W. A. Gardner, "Signal interception: A unifying theoretical framework for feature detection," *IEEE Trans. Commun.*, vol. 36, no. 8, pp. 897–906, Aug. 1988.

[2] R. E. Ziemer and R. L. Peterson, *Digital Communications and Spread Spectrum Systems.* New York: Macmillan, 1985.

[3] D. E. Reed and M. A. Wickert, "A performance comparison of optimum and sub-optimum receiver structures for rate-line detection of digitally modulated carriers," in *Proc. IEEE Region Five Conf.*, 1988, pp. 177–181.

[4] ——, "Minimization of detection of symbol-rate spectral lines by delay and multiply receivers," *IEEE Trans. Commun.*, vol. 36, no. 1, pp. 188–120, Jan. 1988.

[5] ——, "Spread spectrum signals with low probability of chip-rate detection," *IEEE J. Selected Areas Commun.*, vol. 7, no. 4, May 1989.

[6] J. Imbeaux, "Performances of the delay-line multiplier circuit for clock and carrier synchronization in digital satellite communications," *IEEE J. Selected Areas Commun.*, vol. SAC-1, no. 1, pp. 82–95, Jan. 1983.

[7] A. N. D'Andrea and U. Mengali, "Performance analysis of the delay-line clock regenerator," *IEEE Trans. Commun.*, vol. COM-34, no. 4, pp. 321–328, Apr. 1986.

[8] W. A. Gardner, "The role of spectral correlation in design and performance of synchronizers," *IEEE Trans. Commun.*, vol. COM-34, no. 11, pp. 1089–1095, Nov. 1986.

[9] ——, *Statistical Spectral Analysis: A Nonprobabilistic Theory.* Englewood Cliffs, NJ: Prentice-Hall, 1987.

[10] J. F. Kuehls and E. Geraniotis, "Presence detection of binary-phase-shift-keyed and direct-sequence spread-spectrum signals using a prefilter-delay-and-multiply device," *IEEE J. Selected Areas Commun.*, vol. 8, no. 5, pp. 915–933, June 1990.

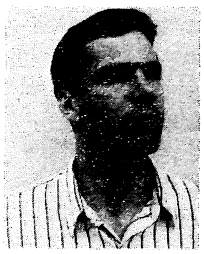

Chad M. Spooner (S'88–M'92) was born in Des Moines, IA, on October 5, 1963. From 1981 to 1984 he attended Santa Rosa Junior College, and was awarded the A.S. degree with high honors in 1984. He received the B.S. degree from the University of California at Berkeley in 1986, and the M.S. and Ph.D. degrees from University of California at Davis in 1988 and 1992, all in electrical engineering.

He was a Teaching Assistant in the Department of Electrical and Computer Engineering at UC Davis from 1986 to 1988. From 1988 to 1992 he was a Research Assistant at UC Davis and a Consultant to Statistical Signal Processing, Inc. He is currently a postgraduate researcher at UC Davis, and is coauthor (with Stephan Schell) of a unique commercially available cyclic spectral analysis software package. His research interests include statistical signal processing, weak-signal detection and parameter estimation, and the theory of higher order cyclostationary signals.

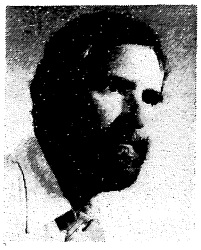

William A. Gardner (S'64–M'67–SM'84–F'91) was born in Palo Alto, CA, on November 4, 1942. He received the M.S. degree from the Stanford University, in 1967, and the Ph.D. degree from the University of Massachusetts, Amherst, in 1972, both in electrical engineering.

He was a member of the Technical Staff at Bell Laboratories in MA, from 1967 to 1969. He has been a faculty member at the University of California, Davis, since 1972, where he is Professor of Electrical Engineering and Computer Science. Since 1982, he has also been President of the engineering consulting firm Statistical Signal Processing, Inc., Yountville, CA. His research interests are in the general area of statistical signal processing, with primary emphasis on the theories of time-series analysis, stochastic processes, and signal detection and estimation and applications to communications and signals intelligence.

Dr. Gardner is the author of *Introduction of Random Processes with Applications to Signals and Systems,* Macmillan, New York, 1985, second edition, McGraw-Hill, New York, 1990, *The Random Processes Tutor: A Comprehensive Solutions Manual for Independent Study,* McGraw-Hill, New York, 1990, and *Statistical Spectral Analysis: A Nonprobabilistic Theory,* Prentice-Hall, Englewood Cliffs, NJ, 1987. He holds several patents and is the author of numerous research-journal papers. He received the Best Paper of the Year Award from the European Association for Signal Processing in 1986 for the paper entitled "The spectral correlation theory of cyclostationary signals," the 1987 Distinguished Engineering Alumnus Award from the University of Massachusetts, and the Stephen O. Rico Prize Paper Award in the Field of Communication Theory from the IEEE Communications Society in 1988 for the paper entitled "Signal interception: A unifying theoretical framework for feature detection," He organized and chaired the NSF/ONR/ARO/AFOSR-sponsored workshop on Cyclostationary Signals, 1992. He is a member of the American Association for the Advancement of Science, the European Association for Signal Processing, and a member of the honor societies Sigma Xi, Tau Beta Pi, Eta Kappa Nu, and Alpha Gamma Sigma.